Applied Catalysis A: General 391 (2011) 158-168

The influence of the nanostructure on the effect of CO_2 on the properties of Pd-Ag thin-film for H_2 separation

S. Abate[a], G. Centi[a,*], S. Perathoner[a], D. S. Su[b], G. Weinberg[b]

[a] University of Messina and INSTM/CASPE (Lab. of Catalysis for Sustainable Production and Energy), Dipartimento di Chimica Industriale ed Ingegneria dei Materiali, V.le F. Stagno d'Alcontres 31, 98166 Messina, Italy
[b] Department of Inorganic Chemistry and ELCASS, Fritz Haber, Institute of the Max Planck Society, Faradayweg 4-6, 14195 Berlin, Germany

[*] Corresponding author: e-mail centi@unime.it,

Received: 12 March 2010; Received in revised form 28 July 2010; Accepted 4 August 2010
Available online 12 August 2010

Dedicated to the friend Helmut Knözinger on in the occasion of his 75th birthday for the seminal contribution to the advancement of fundamental knowledge on catalysis.

Abstract

The use of co-deposition instead of sequential deposition during the preparation of Pd–Ag thin films by electroless plating deposition leads to two different nanostructures, e.g. a dendritic nanostructure or a more compact and dense film, allowing to analyze the role of this parameter, at equal membrane composition, on the performances. In pure H_2 the permeability to hydrogen of the second type of thin films is 3–4 times higher, but the presence of CO_2 in the feed changes considerably the performances. The results are tentatively interpreted on the basis of a non-permanent in situ modification of the characteristics of the Pd–Ag thin films, with creation of strains and microholes particularly enhanced for the nanostructure present in the sample prepared by co-deposition. These strains and microholes are suggested to derive from the combined effect of CO_2 (with creation of subsurface O and/or C) and of hydrogen diffusion through the thin film, which induces lattice expansion and stress on the nanograins. When the flux of H_2 stops, there is a relatively rapid restoring of the initial situation. Scanning electron microscopy (SEM) characterization after the tests in the presence of CO_2 indicates the presence of desintering consistently with above indications and the creation of crack like voids.

Keywords: Palladium; Thin films; Pd-Ag membrane; H_2 separation; Nanostructure; CO_2

1. Introduction

The use of metallic thin films for H_2 separation is becoming of increasing relevance for sustainable chemistry and energy. In fact, the increasing demand of hydrogen has raised exponentially the need of new, more efficient processes for H_2 production by hydrocarbon reforming. Steam reforming of natural gas is a wellestablished technology in refining and fertilizer industries for the production of hydrogen. Due to the thermodynamic limitations in this equilibrium endothermic reaction, the process requires high temperatures (around 900 °C) to have enough methane conversion. However, the process is heat-transfer limited which decreases energy efficiency and causes an exergy loss. An efficient hybrid system (power + hydrogen) with a reduction in energy consumption of about 15% can be realized by using a H_2 membrane separation module downstream of a reforming reactor operating at about 650 °C [1–4]. Advantages in the process efficiency and economics, as well as a reduction of greenhouse gas emissions per kilogram of H_2 produced are thus possible.

A similar concept may also be applied to increase the energy efficiency and process economics of other industrially relevant reactions, such as the catalytic partial oxidation (CPO) of natural gas, the light alkane dehydrogenation to the corresponding alkenes or the water gas shift reaction [5]. Other relevant examples are the use of H_2 permselective membranes in GTL technology to enhance the gasoline yields [6,7] and the integration of H_2 membranes with PEM fuel cells to eliminate poisoning by CO and CO_2 [8]. Pd-based thin films are usually utilized in such a type of H_2 permselective membranes, because ideally (e.g. in defect-free membranes) the selectivity towards

hydrogen is infinite [9–11]. In fact, H_2 catalytically dissociates over Pd and may be transported through the membrane in the form of atomic hydrogen, while the transport of other atoms such as oxygen or carbon virtually does not occur. Therefore, it may be possible to selectively separate H_2 from the complex mixtures such as those produced in the above cited reactions and typically containing carbon oxides, water and hydrocarbons.

Carbon oxides, and in particular CO, have been reported in general to reduce the H_2 permeation rate, although some authors have also indicated that carbon oxides may decompose over Pd membrane surfaces. Li et al. [12] observed CO_2 dissociation above 250 °C yielding molecularly and/or dissociatively adsorbed CO below 400 °C and nanoscopic carbon deposits above 450 °C. Mejdell et al. [13] instead indicated that CO and CO_2 only inhibit surface reactivity of Pd-based membranes, and hence H_2 permeability, by formation of strongly adsorbed species. Nguyen et al. [14] also concluded recently that the effect of CO is only that of competitive adsorption and is fully reversible.

On the other hand, Li et al. [15] reported the formation of a $Pd_{1-x}C_x$ phase in Pd membranes during separation of H_2/CO mixtures, and the reversible incorporation of carbon into palladium. By treatment with H_2 the carbon may be removed. Carbon derives from the dissociation of chemisorbed carbon monoxide. Studying the transient behavior in H_2 permeance of Pd-based membranes after stopping the feed of CO_2, Gielens et al. [16] found that carbon dioxide has a more complex effect than that of simple competitive chemisorption.

Therefore, the H_2 permeance of Pd-based thin membranes is affected from the catalytic processes occurring on the surface, although there are discordances in literature about the effective nature of these effects, e.g. whether only competitive strong chemisorption, or instead phenomena related to the dissociation of carbon oxides. In general, the possibility of having diffusion of C and/or O in the Pd membrane is not considered, but in few cases the possibility of C diffusion has been reported.

In the catalysis area, it is well established that on Pd nanoparticles there is the possibility to have subsurface C and that this subsurface carbon may significantly influence the surface reactivity of Pd [17–19]. Low-coordinated Pd atoms, present at the nanoparticle edges, facilitate the formation and diffusion of carbon into tetrahedral subsurface sites. On these sites the reaction is almost non-activated [20]. Therefore, on smaller and more defective Pd nanoparticles the formation of subsurface C is enhanced. It is also known that subsurface O in Pd nanocrystals can influence the surface reactivity [21,22].

The question is thus whether these observations on small Pd nanoparticles could be relevant also to interpret the effect of carbon oxides on the performances of Pd-based thin films, e.g. whether subsurface diffusion of C and/or O could occur after carbon oxides dissociation and the related influence on the surface reactivity of the membrane. We should comment regarding this aspect that Pd-based thin films could be prepared by different preparation methods, but a common method is by electroless plating deposition (EPD) [23–26]. The method used in this work is based on the decomposition of hydrazine over metallic Pd seeds. The electrons generated in this reaction give rise to in situ reduction of Pd^{2+} to Pd^0 forming metallic Pd nanoparticles with a dendritic growing up to finally giving rise to a compact thin metallic film [27,28]. However, due to the mechanism of formation, the film should be better described as a dense assembly of nanograins.

Usually, to enhance the performances and especially the stability of Pd-based thin films, alloys with Ag, Cu or other elements (Au, Ru, etc.) are prepared [29,30]. Pd–Ag membranes, with a typical silver amount of 23 wt.%, are among the most common used. In these bimetallic thin films, two main variations in our preparation method by EPD could be cited: co-deposition and sequential deposition [25,31,32] of Pd and the second metal (Ag, in our case). These two methods lead to a different nanomorphology, the sequential method leading preferentially to a relatively dense and flat membrane, while the co-deposition gives preferentially a dendritic nanostructure. Therefore, thin films prepared by these two methods would have similar characteristics, but a different nanostructure. We suggest that they could act as a good model to understand the role of the surface nanostructure on the catalytic reactivity of the thin film, and the relevance of eventual subsurface O and C species on the surface reactivity and performances.

These effects are of more general value also for catalysis. In fact, the research interest on the use of these Pd-based thin films as catalysts is increasing. We reported in the past the use of these membranes for the catalytic selective reduction of nitrate in ground water [33]. Later, various authors have also investigated similar catalytic membranes for removing nitrates from groundwater [34,35]. We also used these membranes for the direct synthesis of H_2O_2 from H_2 and O_2 [36,37], and recently other research groups have investigated them in the same reaction [38,39]. Very interesting results have been also obtained using similar membranes for the catalytic direct oxidation of benzene to phenol [40–43]. In this system, the active oxygen species is formed on the surface of Pd via the reaction between oxygen and permeated hydrogen from opposite sides of the membrane. Hydroxylation occurs on the surface of Pd via reaction of the aromatic compound and active oxygen. Also in this case, the formation of subsurface C and/or oxygen species may possibly have a significant role on the surface reactivity. In fact, recent results have indicated that improved performances in the benzene direct hydroxylation could be obtained in Pd membranes prepared by EPD which leads to nanostructures characterized from an assembling of Pd nanograins. Benzene direct hydroxylation to phenol, in alternative to the three step commercial process, is industrially attractive as novel sustainable process, because it potentially allows a significant decrease in energy consumption and production of wastes, as well as an improvement in process safety [44].

Therefore, the surface reactivity of the Pd-based thin film could be affected by the presence of subsurface spe-

cies and this effect is potentially relevant in their use both as membrane and catalysts. On the other hand, it is unclear whether the specific type of nanostructure of the Pd-based thin film has a role. However, classical methods for surface studies are not well suited to understand this question, because hydrogen absorbed in Pd thin films causes a lattice expansion [45] and this affects the subsurface diffusion of other species in palladium [46]. Therefore, in the absence of a flux of hydrogen through the thin film, not reliable data could be obtained.

Thus, we approached this question by comparing the behavior, particularly in terms of possible diffusion of C and/or O species through the palladium layer, of two thin film Pd–Ag membranes prepared with the same composition, but using co-deposition or sequential deposition EPD methods. As will be shown here, the first thin film is characterized from a dense assembly of nanograins and dendritic nanostructure, while the second from a dense and amore compact film structure. Their comparison will allow to analyze the effect of the presence of amore defective nanostructure on the formation and diffusion of subsurface C and/or O species, and how this effect influences the surface reactivity and hydrogen permeability.

The scope of this manuscript is thus to evidence how a change in a preparation method for Pd-alloy thin film membranes, e.g. the use of a co-deposition instead of sequential deposition, leads to a significant change of the nanostructure of the Pd–Ag thin film. This change has relatively minor impact on the H_2 permeability with pure H_2. On the contrary, the tests in the presence of CO_2 evidence a significant change in the performances (time-on-stream dependence of the permselectivity in long term experiments, shows the influence of CO_2 on hydrogen permeance). This effect is not permanent and is tentatively interpreted as the formation of reversible microholes, associated to strains and microholes deriving from the combined effect of CO_2 (with creation of subsurface O and/or C) and of hydrogen diffusion through the thin film, which induces lattice expansion and stress on the nanograins.

Even with the limitations in passing from a thin film to discrete (dispersed) Pd-based nanoparticles, it may be suggested that this kind of phenomena are more general, and a relevant aspect to investigate is to determine the properties of supported Pd-based catalysts.

2. Experimental

2.1. Preparation of the Pd–Ag supported thin films

Asymmetric porous α-Al_2O_3 tubes (final layer porosity 70 nm) provided by INOPOR, Germany, were used as the substrate for the deposition of Pd-based thin films [26,47–49]. The ceramic support is first cleaned from grease and other contaminations using purified isopropanol and then is dried at 100 ◦C for 3 h. A thin film of Pd–Ag (23 wt.% Ag) was then deposited on these membranes by EPD method. The EPD technique consists of two main consecutive steps: (i) first Pd-based nanocrystals (seeds) are created on the membrane surface (seeding or activation step), and then (ii) deposition of Pd–Ag layer occurs by reduction of Pd and Ag ions present in an aqueous solution in contact with the inner part of the alumina tube using the electrons generated in the decomposition of hydrazine over the Pd-based nanocrystals. The seeding procedure was described in detail before [26]. Two different procedures were used for this second step.

Table 1: Composition of the plating bath used in the preparation of M1 and M2 Pd–Ag thin films supported over ceramic alumina tubes.

Chemical	M1	M2	
	$Pd_{77}Ag_{23}$ bath	Pd bath	Ag bath
$PdCl_2$ (g/l)	5	5	–
$AgNO_3$ (g/l)	1.24	–	1.24
EDTA (g/l)	40	30	14
NH_4OH (25%) (ml/l)	290	290	290
N_2H_4 (1 M) (ml/l)	10	10	10
Bath temperature (°C)	50	40	40
pH	11	11	11
Time (h)	20	20	6

2.1.1. Simultaneous deposition (co-plating)

Pd and Ag were simultaneously deposited onto the porous support prior to be activated by direct impregnation of the palladium complex followed by reduction with hydrazine. The typical composition of the used plating bath is reported in Table 1. The procedure could be repeated several times in order to increase the thickness of the deposited Pd–Ag film. This membrane was called M1.

2.1.2. Sequential deposition

In the sequential procedure Pd an Ag layers were deposited consecutively. After surface activation palladium and silver depositions were performed using a bath composition shown in Table 1. After each deposition, the membrane was rinsed with deionised water, and then dried in an oven at 80 ◦C for 2 h. This membrane was called M2.

The M1 and M2 membranes were finally treated in N_2 flow for 5 h at 500 ◦C.

2.2. Characterization of the Pd–Ag supported thin films

The Pd–Ag supported thin films have been characterized by atomic force microscopy (AFM), scanning electron microscopy (SEM), electron-dispersive X-ray emission (EDX) mapping before and after reactivity tests. AFM characterization has been made using a Perception SPM from Assing (Italy), using contact mode operations. The tip used

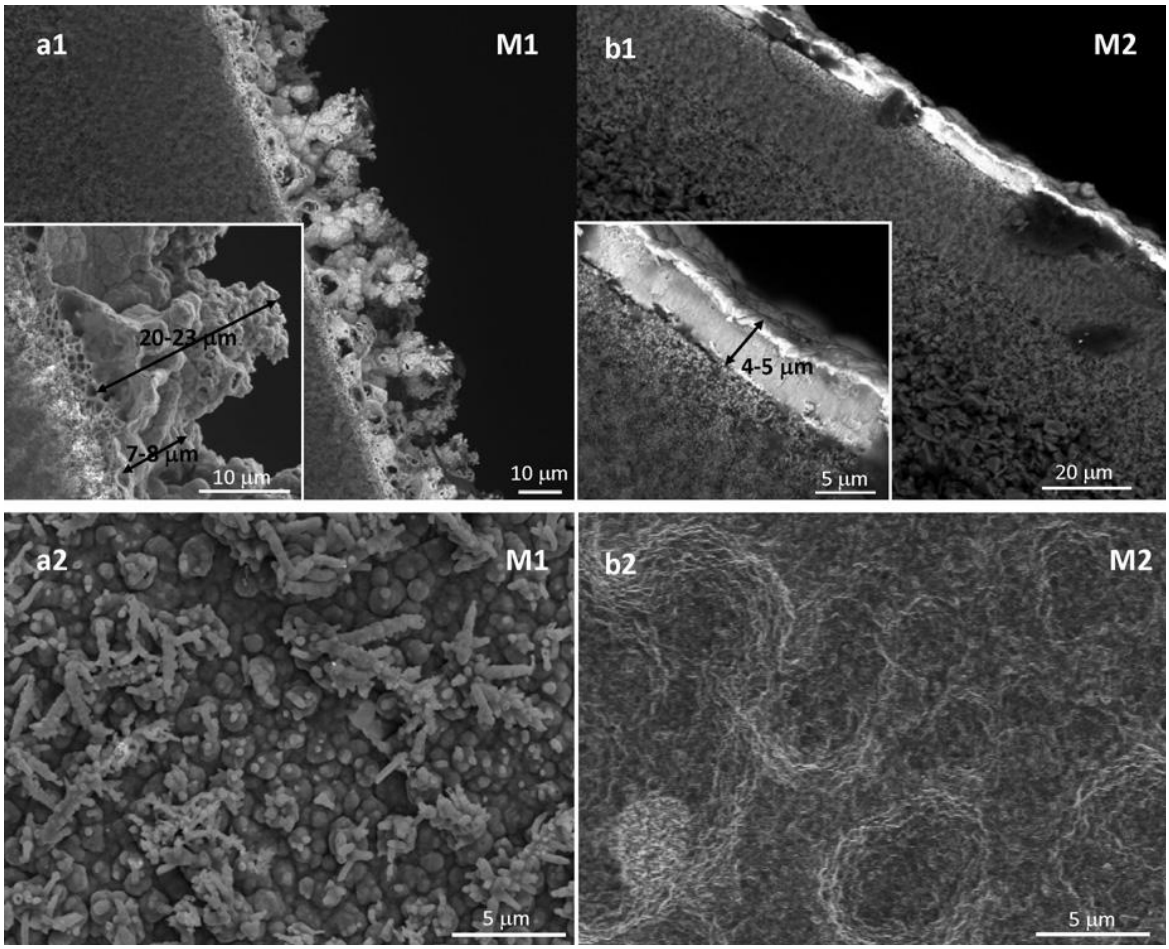

Fig. 1: SEM images of M1 (a1, a2) and M2 (b1, b2) thin films. Cross section (a1, b1) and top view (a2, b2).

was silicon nitride (Veeco), with a level 0.5N/m Au Reflex coating. EDX–SEM characterization studies of the membranes were made with a scanning electron microscope Jeol 5600 LV (HV15kV). Elemental analysis was carried out via energy dispersion analysis using an X-ray analytical system EDX OXFORD, coupled to the scanning electron microscope.

After membranes preparation the bubble point method was used to locate possible defects and pinholes, immersing the membrane in an ethanol/water mixture. Moreover, leak tests were made in order to analyze both the sealing of the graphite rings and the presence of cracks in the membrane, by pressuring the membrane with He up to a pressure of 9 bar, about 1.5 times higher than the maximum pressure used in permeability studies. No measurable flux (minimum detectable flow is 0.04 ml/min), using a Bronkhorst digital massflowmeter (accuracy is±0.8% reading,±0.2% full scale) in the permeate side has been detected working at high temperature (about 450 ˚C), before starting the separation tests. These tests were repeated at the end of experiments. Note that this method gives only indications about the presence of relatively large holes.

Permeability tests have been made in the stainless steel reactor (permeator) earlier described [26]. Both annular ends between the membrane tube and the permeator wall were sealed with moulded graphite rings. The permeator was placed in an electrical furnace and heated to the desired temperatures (range 350–450 ˚C).

A K-type thermocouple within the membrane tube was used to control the temperature during the permeation experiments. All gases were introduced into the permeator using a calibrated multichannel mass-flow controller. The inlet feed was connected to the inner side of the membrane and the permeated gases were measured on the outer side of the membrane, at atmospheric pressure. No sweep gas has been used. The pressure in the inner side of the tube was monitored via a pressure controller.

The permeation behavior of the membrane was measured with pure H_2 at three different temperatures in the 350–450 ˚C range. Tests were made analyzing the H_2 permeate flux as a function of time at fixed temperature and transmembrane pressure differential. A stable behavior is typically observed after few hours, but in some cases the time of the test was extended to have better indications on stability of operations. Then pressure differential across the membrane is increased (ΔP in the 0.5–5 bar range) and the flux of H_2 monitored again as a function of time-on-stream.

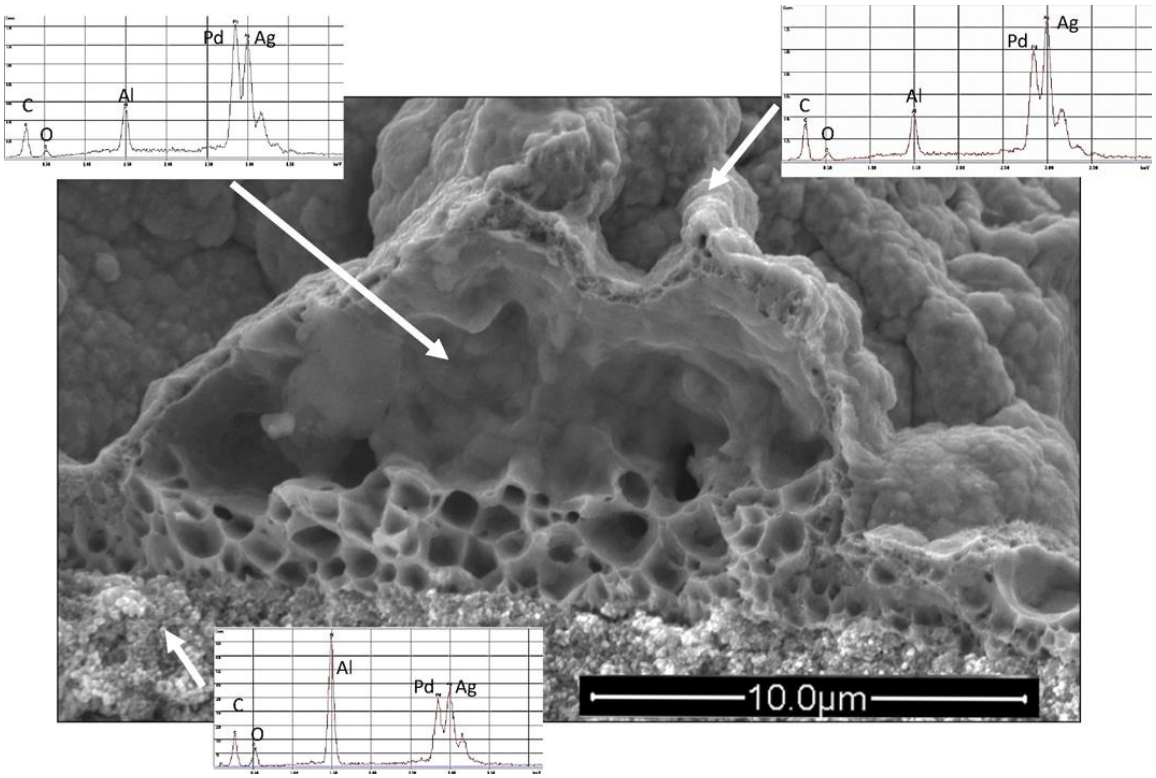

Fig. 2: SEM image of M1 thin film with EDX microanalysis of different areas.

The tests with a H_2:N_2:CO_2 feed were made in the same experimental apparatus. In these tests, the amount of CO_2 in the feed was changed between 10% and 20% at two different temperatures (400–450 ˚C), while total pressure differential across the Pd–Ag thin film was maintained constant at 2 bar. The flow rate of either permeate or feed gas were measured by a Bronkhorst digital mass flow meter, and feed mixture and permeate compositions were analyzed using a gas chromatograph (Agilent 3000A equipped with a Molsieve 5A column using Argon as carrier gas).

In these tests, the permeate flux was monitored as a function of time-on-stream for about 25–30 h, before the feed composition or the temperature were changed, and the permeate flux was monitored again as a function of time-on-stream for about 25–30 h. The membrane has been maintained in pure nitrogen flow for about 0.5–1 h between these consecutive tests, in order to stabilize the temperature or prepare the new feed composition. This time lag in pure nitrogen flow has been omitted in the figure summarizing the results (see later).

3. Results and discussion

3.1. Characterization of the Pd–Ag thin films

SEM images evidence that the preparation by co-deposition (M1) leads to a thin film characterized from a dendritic structure with faceted crystallites (Fig. 1, a1—cross section, a2—top view). This effect is due likely to the different growth modes of Pd and Ag grains during electroless deposition. It has been observed that Ag is preferentially deposited on the Pd seed nuclei, and therefore Ag tends to shield active Pd particles and inhibits the plating reaction [50]. The resulting Pd–Ag layer is macroscopically homogeneous (by EDX mapping), but shows a significant roughness as shown in Fig. 1 and at nanoscale level the composition may result inhomogeneous.

The film results thus as a dense assembly of nanograins with size ranging from 100 to 300 nm, having a core rich of Pd and an outer shell rich in Ag. The film thickness varies from 7–8 to 20–23_m(see inset in Fig. 1(a1)). Fig. 2 reports a largeSEMimage of the film which evidences that the inner part of the thin film has a sponge-like nanostructure, but apparently with limited or even absent connectivity between the voids and a denser top layer of thickness 200–300 nm.

EDX analysis evidences that the outer surface is richer in silver, while the inner part richer in Pd (Fig. 2).

The thin film prepared by sequential deposition (M2) (Fig. 1(b1) and (b2), cross section and top view, respectively) shows a homogeneous layer with a lower roughness than M1, and a higher compactness of the films. Although the cross section image (see inset in Fig. 1(b1)) suggests the presence of a relatively flat surface, the top view (Fig. 1(b2)) evidences the presence of grains, which are significantly larger than those in the case of M1 thin film.

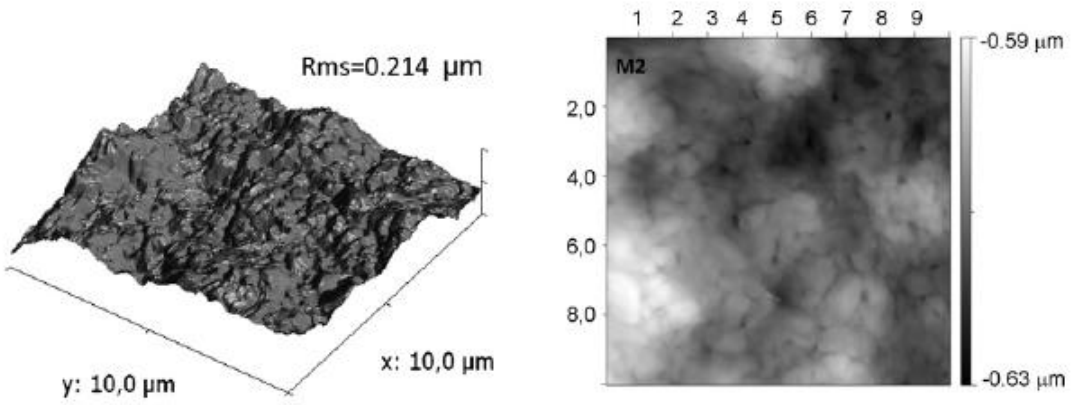

Fig. 3: AFM mapping of the surface roughness and nanomorphology of M2 thin film.

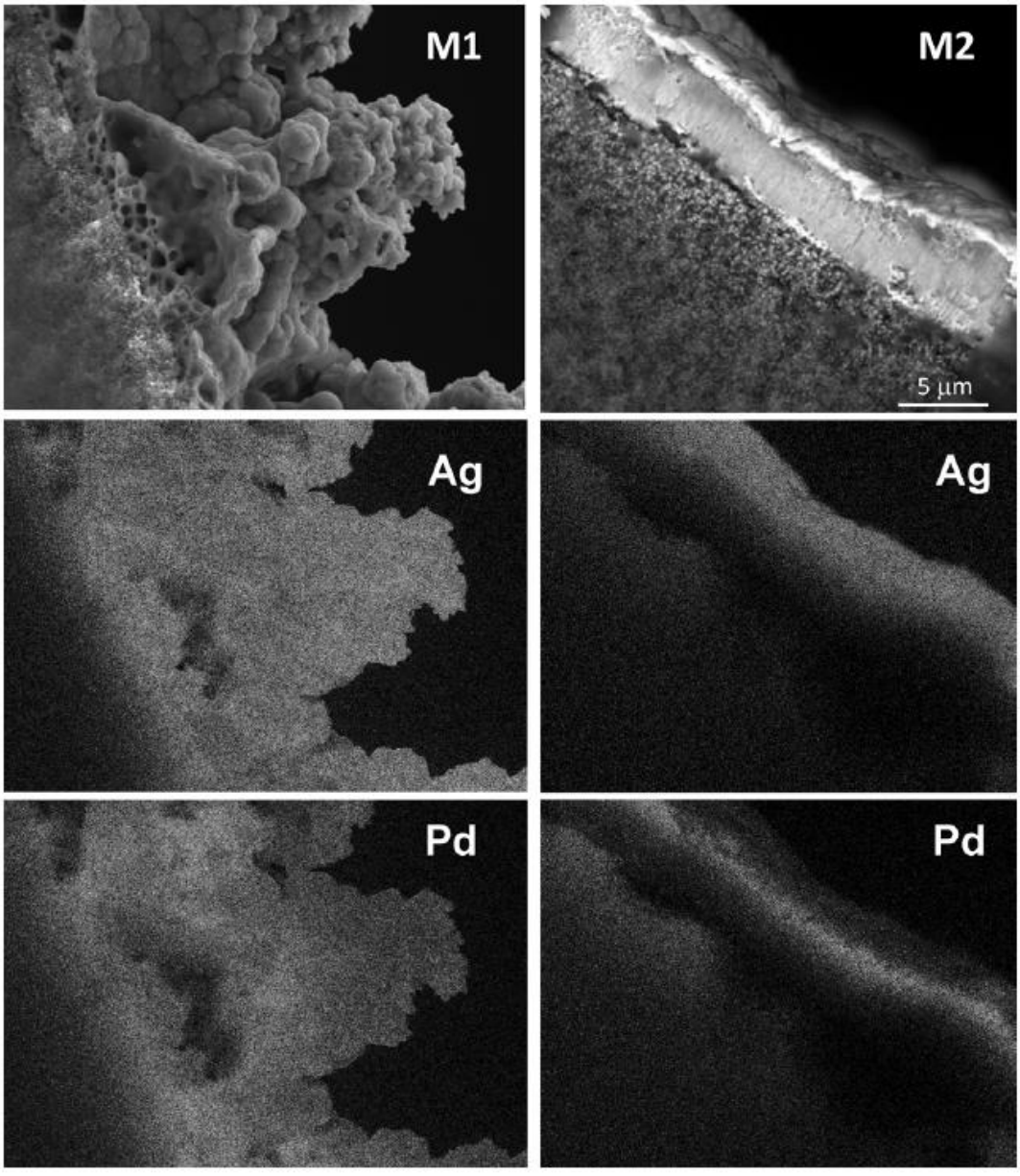

Fig. 4: SEM images of the cross section of M1 and M2 thin films, and relative mapping of Ag and Pd obtained by EDX analysis.

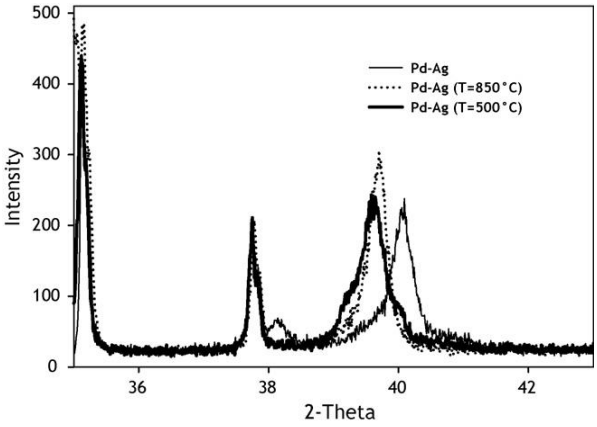

Fig. 5: Comparison of the XRD patterns of Pd–Ag thin films after the plating stage and after the consecutive annealing in N_2 flow at 850 or 500 ˚C.

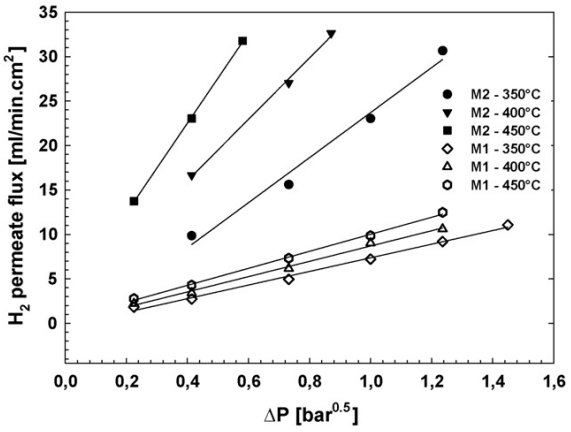

Fig. 6: Relationship between hydrogen permeation flux and the difference in the square root of hydrogen pressure between the tube-side and the shell-side (ΔP) at different temperature for M1 and M2 thin films.

AFM images of the sample (Fig. 3) confirm the presence of grains with mean size of 0.5–1μm and a mean surface roughness (Rms) of about 0.2μm. Due to the high surface roughness, it is not possible to analyze by AFM the M1 sample, but the SEM images (Fig. 1(a1) and (a2)) clearly evidences the presence of an order of magnitude higher roughness (Rms over 5μm) and a one order of magnitude lower mean dimension of the grain size. Fig. 4 reports the mapping of Pd and Ag (by EDX–SEM) in the two M1 and M2 thin films. While the M1 sample shows an apparent homogeneous distribution of Pd and Ag, although with the local differences remarked before (see Fig. 2), the concentration of Ag in the top layer of this film is evident for M2 sample. This is in agreement with the sequential deposition method. In both thin films there is preferentially Ag on the surface, but due to the presence of smaller nanograins in M1 an apparent better distribution is present.

From the characterization of M1 and M2 thin films we may conclude that the change from co-deposition to sequential deposition of Pd and Ag during the preparation of these materials by EPD method leads mainly to the formation of one order magnitude smaller nanograins and higher surface roughness due to the dendritic growing which is accentuated in M1 sample. The consequence is also a different degree of compactness of the two thin films. In both cases there is a surface enrichment in Ag at the level of grain size, although on a large scale the M1 sample appears more homogeneous in terms of Pd and Ag distribution.

We feel, however, that this is a consequence of the different nanostructure. We have not conclusive evidences, whether at the grain level the surface is richer in Ag in M2 case with respect to M1. On the other hand, surface techniques such as XPS have not the necessary spatial resolution to provide reliable indications. By EDX local mapping, there are limited differences at the interface region (grain boundaries), but this technique is only indicative. We could thus suggest that the main difference between the two samples is the nanostructure in terms of grain assembling, being M1 characterized from smaller grains and a more open dendritic arrangement. M2 has one order of magnitude larger grains and a dense and compact flat-type arrangement. Silver is preferentially located at the surface of grains.

Note finally, that the characteristic morphology of the M1 thin film is not a consequence of an insufficient annealing. The X-ray diffraction (XRD) patterns of the Pd–Ag thin film obtained after EPD (Pd–Ag), and after annealing at 850 ˚C (Pd–Ag T = 850 ˚C) or 500 ˚C (Pd–Ag T = 500 ◦C) in N_2 flow are reported in Fig. 5. The film immediately after plating (Pd–Ag) consists of individual Pd and Ag seeds without formation of the Pd–Ag alloys. The annealing in nitrogen at 500 ˚C gives rise to the formation of the Ag–Pd alloy as shown from the shift of the (1 1 1) reflection of Pd from about 2Θ= 40.1–39.78 (Pd–Ag) and the simultaneous disappearance of the Ag reflection at about 38.18. Further annealing at higher temperature (850 ˚C) does not further change the situation, leading instead to the creation of large amounts of cracks and defects on the thin film.

3.2. Permeability to H_2 of the thin films

The results, for permeation with pure H_2, are reported in Fig. 6 at three different temperatures in the 350–450 ˚C range.

Tests were made analyzing the H_2 permeate flux as a function of time at a fixed temperature and transmembrane pressure differential. After reaching a stable H_2 permeate flux, the pressure differential across the membrane is increased (ΔP in the 0.5–5 bar range) and the flux of H_2 monitored again as a function of time-onstream. The results reported in Fig. 6 indicate that the permeation rate of H_2 is directly proportional to $\Delta P = P_f^{0.5} - P_p^{0.5}$, e.g. the difference in the square roots of hydrogen pressures between the

feed (f) and the permeation (p) sides of the thin membrane film. This is consistent with Sievert's law [51]:

$$J_{H_2} = \frac{Q}{\delta}(P_f^n - P_p^n) \quad (1)$$

where J_{H2} is the transmembrane flux of H_2, Q the permeability and δ the thickness of the Pd–Ag membrane. The exponent n varies between 0.5, when the rate-limiting step is the bulk transport of hydrogen across the thin metallic film, to 1.0, when the surface dissociation of hydrogen is the limiting step [52].

Table 2 summarizes the dependence of the permeance from the temperature on the two thin films M1 and M2. The values of R2 obtained during the linear regression are also reported, which give an indication of the good fitting of the data.

Table 2: Permeance as a function of the temperature for M1 and M2 thin films and values of R2 in linear regression of the data reported in Fig. 5.

T(°C)	$Q/\Delta z$[cm min^{-1} bar$^{-0.5}$]		R^2 (from linear regression)	
	M1	M2	M1	M2
350	7.28	23.24	0.9925	0.9783
400	8.84	38.20	0.9945	0.9889
450	10.53	57.13	0.9947	0.9887

The H_2 permeability of the two thin films is in agreement with the values reported in literature, taking into account the difficulty in comparing the results due to the wide range of reaction conditions used [52–54]. Obtaining the permeance by dividing the permeability by the membrane thickness is formally correct only for a compact (homogeneous) layer. In our case, quite different characteristics of the thin films are present. Even with this limit, it is useful to have a rough estimation of the permeability and activation energy in the two membranes.

The experimental values of H_2 permeance (Q/δ) at different temperatures were used to estimate the activation energy for H_2 permeation, using an Arrhenius plot (Fig. 7). For both samples there is a good linear fit of the data, with a value of the regression coefficient (R2) of 0.998 and 0.994 for M1 and M2 samples, respectively.

The activation energy of the M1 thin film was found to be 17.5 kJ/mol, while that of M2 42.8 kJ/mol. The lower value for M1 tentatively suggests that amixed mechanism of hydrogen transport through the membrane could be present.

To note that the M2 membrane has characteristics close to those often reported for dense thin-film Pd-based membrane, while the M1 membrane show a very high surface roughness and a dendritic nanostructure which makes from one side less precise the estimation of the permeance and activation energy, and from the other side has a probable influence on the mechanism of transport. We tentatively suggest that the difference between the M1 and M2 mem

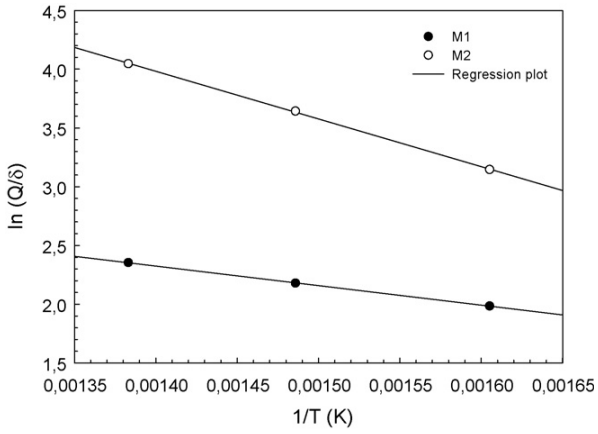

Fig. 7: Arrhenius plot of the relationship between the H_2 permeance and temperature in M1 and M2 thin films.

branes could be related to the presence in M1 of a mixed diffusion mechanism (grain and intergrain, see later) and this is the cause of the low activation energy [26]. However, this is an aspect which deserves more studies.

In conclusion, permeability tests to H_2 of the two thin films M1 and M2 indicate that M2, due to the more uniform and lower mean thickness shows a higher permeate flux of H_2 at the same conditions. However, the permeance (the permeability divided by the mean film thickness) in the studied temperature range is not very different. If fact, the mean film thickness may be estimated to be around three times larger in M1 with respect to M2 thin film, but particularly for the M1 sample the great uncertainly on the value, due to the characteristic nanomorphology of the film (Fig. 1), do not allow more precise estimations.

The more than twice value of the activation energy for hydrogen diffusion in the film for M2 sample suggests a difference in the H transport through the film. Being the composition and experimental conditions the same, we believe that the possible explanation is related to the different nanostructure of the film. The interface region between the grains, where silver is predominant, is higher in the M1 sample, due to the presence of significantly smaller grains. Therefore, diffusion in the boundary region between grains [55] with respect to the classical bulk diffusion mechanism in Pd [23] could be enhanced. Similarly, the presence of nanovoids, although not connected each other's or with the surface, will affect the transport mechanism.

Barlag et al. [56] reported that the macroscopic hydrogen diffusion coefficient in homogeneous $Pd_{1-x}Ag_x$ alloys remains nearly constant up to silver concentrations of about 25%. Then it falls off reaching a minimum value at 60% silver content before increasing again with rising silver content directly towards the value for pure silver, which is nearly the same as for Pd. At smaller silver contents the silver atoms partly block the energetically favored diffusion paths in the Pd matrix leading to round-about way diffusion. At high silver concentrations, Pd atoms act as traps for hydrogen in a silver matrix. The interplay of the hydrogen transport via two kinds of occupation sites with differ

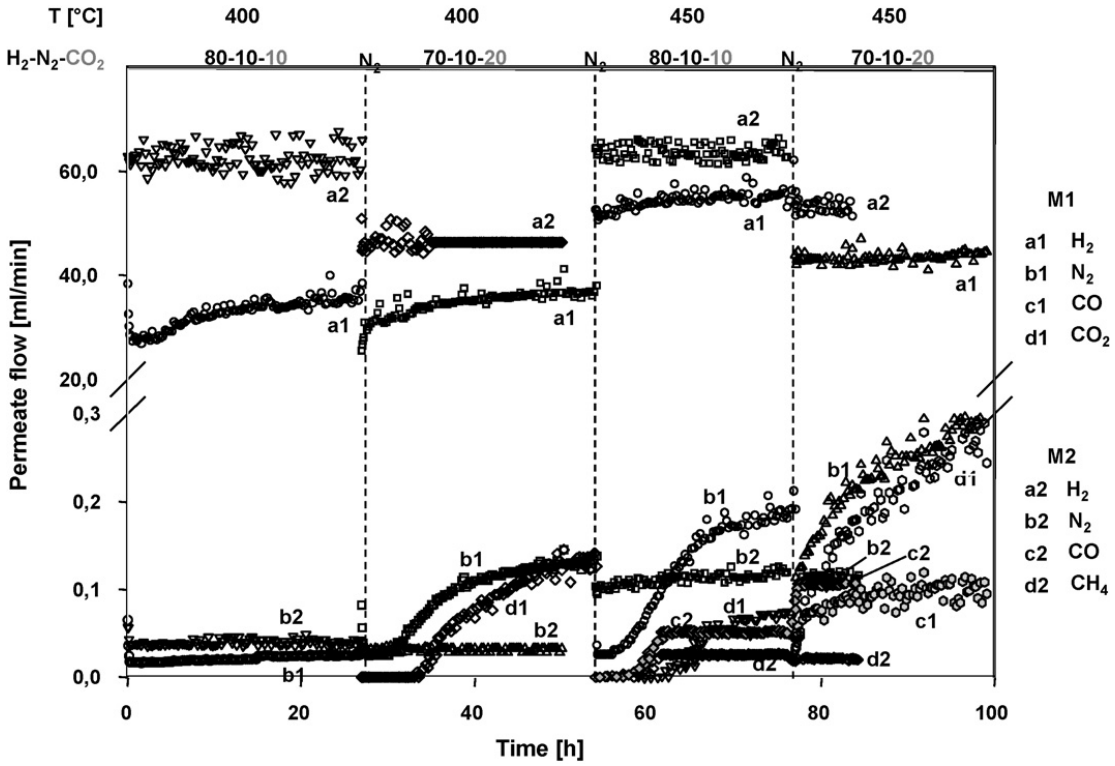

Fig. 8: Flux of H_2 and other components in the permeate side as a function of time-on-stream during a sequence of experiments feeding mixtures of H_2:N_2:CO_2 at 400 and 450 °C on M1 and M2 thin films.

ent hydrogen solubility determines the shape of the curve for the macroscopic diffusion coefficient as a function of the alloy composition. Therefore, in silver-rich intergrain regions, hydrogen could efficiently diffuse, but through a different mechanism with respect to that present in pure Pd or Pd–Ag alloy, when the Pd/Ag ratio is above four.

3.3. Influence of CO_2 on the transport of H2 through the thin films

Fig. 8 reports the permeate flux of H_2 and other species detected on the permeate side of the thin film as a function of time-onstream for both M1 and M2 samples. The behavior is monitored for about 25–30 h of time-on-stream, before to change the feed composition and/or the temperature, as indicated in the figure. Note that the samples have been maintained for about 0.5–1 h in inert gas flow (N_2) during each of these changes, but for conciseness this time lag has been not included in Fig. 8. The feed in these tests is composed of principally H_2 plus N_2 and CO_2 in variable amounts (in the 10–20% range). We use a high retentate flow rate coupled with the Pd–Ag deposited in the inner part of the ceramic membrane to have a turbulent flow which together with a low degree of conversion of H_2 and other gas components suggests the absence of polarization effects [57], although computer fluidodynamic simulations (CFD) would be necessary for more precise conclusions. To note also that the time to reach stationary retentate composition is less than 1 h. Therefore, the transient effects observed (on a time scale of hours) are not determined from the transient related to establish uniform composition. This conclusion is supported from the fact than in M2 membrane the nearly stationary composition at 400 °C in the permeate membrane side establishes within less than about 15 min (see below).

The analyses of the retentate-side flow at the outlet of the membrane reactor indicate that still hydrogen is in very large amount and that neither CO nor CH_4 could be detected, except traces. Note that retentate indicates the portion of the feed that does not pass through a cross flow membrane, while permeate is the part of the flow that passes through the membrane. The results in Fig. 8 refer to only the permeate flux of H_2 and other species. Note also the change in scale in Fig. 8 y axis.

The observation that COand CH_4 are detected only at the permeate side and not at the retentate side (absence or presence in very low amounts), indicates that they cannot be associated to a simple transport by Knudsen or viscous flow transport through holes in the thin film. This conclusion is also supported from the observation of the time-on-stream behavior. For example, in the tests at 450 °C (H_2:N_2:CO_2 = 80:10:10), the formation of CO and N_2 slowly grows with time-on-stream in M1 thins film, differently from M2 thin film.

A possible interpretation of this effect is that with time-onstream nanoholes form and this effect causes a progressive increase in the amount of N_2 and CO being trans

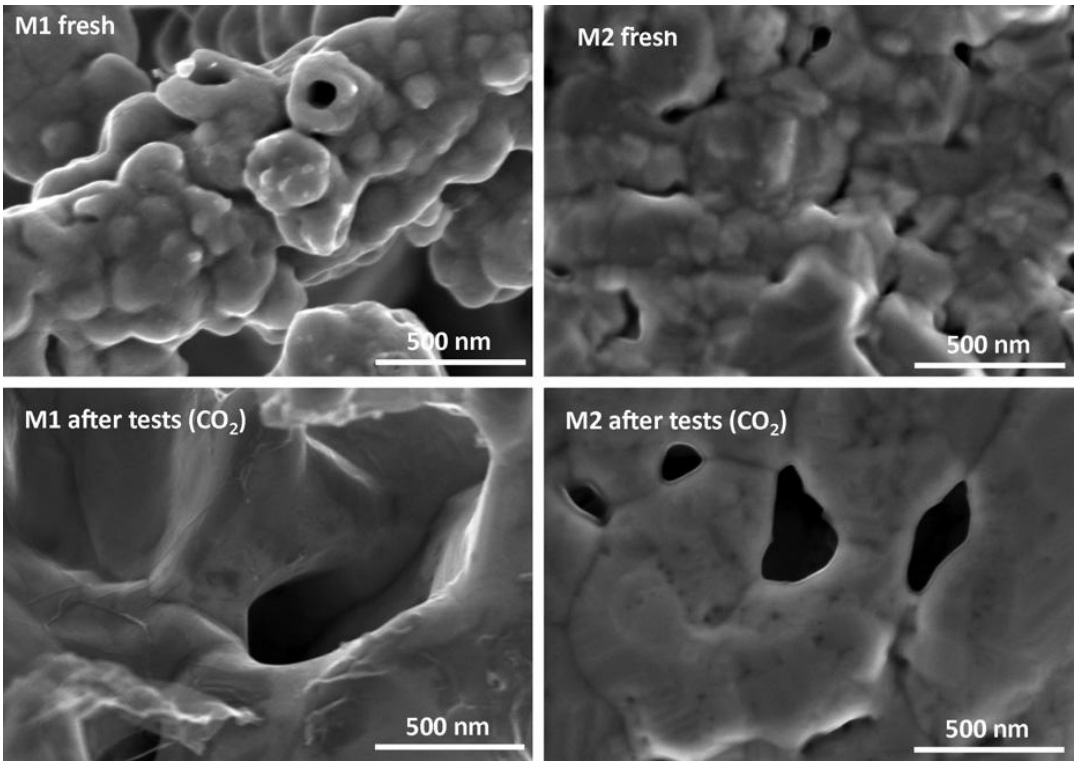

Fig. 9: SEM images of M1 and M2 thin films before (fresh) and after the tests with the presence of CO2 in the feed.

ported through the film by Knudsen diffusion or viscous flow. CO is not detected in the retentate side, but may derive from the decomposition of CO_2 during the transport through the film. According to this interpretation, it should be a permanent modification of the thin film and thus the initial amount of the same species during the consecu tive experiments at higher temperature (450 ◦C) should be equal or higher than the final amount observed at 400 ˚C. On the contrary, we observed that the initial amount is very low, and then grows again with time-on-stream. Changing the feed composition at the same temperature, the initial amount is again initially low and then grows with time-on-stream. Note that during these switches in the experimental conditions the membrane is kept in the reactor at the same temperature, but in inert (N_2) flow. Therefore, the results do not indicate an effect of permanent modification of the membranecharacteristics. On the other hand, the effect in M2 membrane is not present at 400 ◦C and at 450 ˚C for the 10% CO_2 concentration in the feed, but it is present at 450 ˚C for the 20% CO_2 in the feed. This result clearly evidences that the effect cannot be attributed to the time to establish an equilibrium through the membrane and within the membrane reactor.

One possible interpretation could be related to reversible strains in the thin film nanostructure which derives from the lattice expansion caused from hydrogen diffusion through the thin film. This is reasonably a slow process, and thus a time from 10 to 20 h could be necessary to fully develop. During the time lag between the two consecutive experiments, the reduction of hydrogen partial pressure (e.g. the use of N_2 flow) would reduce the amount of hydrogen present in the thin film, and as a consequence these nanoholes close again. The alternative explanation is the presence of dissociation of N_2 and CO_2 at the retentate side, transport of the atoms through the thin film and then recombination at the permeate side. Possibly a combination of the two effects could be present.

The nanostructure of the thin film has a significant role on these effects. In fact, the slow growing of N_2 and carbon oxides is generally observed in all the consecutive tests for M1 sample, apart from the initial ones at the lower temperature and CO_2 concentration in the feed. On the contrary, the amount of these species in the permeate side is generally constant with time-onstream for all the tested temperatures and feed compositions in the case of M2 thin film. The presence of nanograins and a less dense nanostructure inM1thus favor the presence of the described phenomena.

The presence of CO_2 significantly influences the behavior of the thin M1 and M2 films, but in a different way depending on the nanostructure. In fact, in pure H_2 at 400 ˚C, the flux of H_2 passing through the M2 thin film is about three times that through M1 film (Fig. 6). However, in the presence of 10% CO_2, the difference is reduced to about 1.1–1.5, and to 1.1–1.2 for 20% CO_2 (Fig. 8). At 450 ˚C the effect is even larger, reducing from over 4 to about 1.1. It may be also noted that at 400 ˚C the increase of CO_2 concentration from 10% to 20% has no effect on the H_2 permeate flow of M1, while it reduces the H_2 permeate flow of M2 by 20%. This observation is not consistent with the

hypothesis of only a competitive chemisorption of CO_2 on the sites for H_2 dissociation.

It is possible also to note that at 400 ◦C, the flow of H_2 through the M1 thin film increases by about 15% during about 25 h of time-onstream, while it is constant in the case of M2 thin membrane. The effect is present both using 10% and 20% CO_2 in the feed, although in the latter case, the increasing concentration of N_2 and CO_2 in the permeate side (in small amounts) is detected differently from the case using 10% CO_2. This effect is instead not present using the M2 thin film, where the low and constant amounts of N2 are related to only some leakage of N_2 from atmospheric air in the pipe to the analysis system.

At 450 ◦C the situation is more complex, because in both M1 and M2 thin films the increase of CO_2 causes a lowering of the H_2 permeate flux, although as mentioned above, the two samples have very close performances, despite the four times different behavior in pure H_2. Other differences are the following:

- The N_2 amount in the permeate side for M2 thin film is constant, while increases in the case of M1 sample.
- CH4, although in very low amounts, is observed for M2 sample, but no CO_2, as for M1 sample.
- CO is observed in both M1 and M2 cases (at the higher temperature and CO_2 concentration), but the amount is essentially constant for M2 sample, while grows with time-on-stream for the M1 sample.

In conclusion, the two M1 and M2 thin films have a quite different sensitivity in the presence of CO2 in the feed and their time-on-stream behavior shows differences which cannot be explained only on the basis of a competitive chemisorption of CO_2 on the surface and an inhibition of hydrogen dissociation. Note also that in both cases no evidence have been found, after separation tests, of the presence of carbon species on the surface of the thin film (see later), at least at temperatures equal or below 450 ◦C. The detection of CO in the permeate is indicative of the presence of dissociation of carbon dioxide, but this effect is present only in the tests at 450 ◦C and not at 400 ◦C (Fig. 8).

At 400 ◦C the main difference between the two thin films is that M1 apparently has less sensitivity to CO_2, and that the flux of hydrogen passing through the thin film increases with the timeon- stream, although the effect is reversible. In fact, after changing the feed composition from 10% to 20%CO_2 (during the change in the feed composition, the sample is maintained in flux of N_2 for about 0.5–1 h), the flux of H_2 starts again from a lower value increasing later with the time-on-stream. Note that the process of hydrogen diffusion through a Pd thin film is fast enough to be not seen on the time scale of the experiments reported in Fig. 8. In agreement, in the case of M2 sample, no effect is observed and the H_2 flux through the thin film maintains constant with time-on-stream. The effect observed for M1 sample should be thus associated to a reversible modification in the thin film characteristics, and reasonably to the different nanomorphology and nanostructure with respect to M2.

A possible explanation is the formation of strains and microholes associated to expansion of the lattice due to H_2,which should be enhanced in M1 sample with respect to M2, and may be a reversible effect as commented before. However, this explanation is in contrast with the observation of the three times higher hydrogen permeability of M2 with respect to M1 using pure H_2 (Fig. 6), and the much reduced difference in behavior when CO_2 is present. In addition, the increase in the flux of hydrogen for M1 sample was not observed using pure H_2 in the feed. Therefore, the formation of strains and microholes occurs when CO_2 is present in the feed and probably is associated to a partial decomposition of CO_2 and subsurface O and/or C diffusion. Although CO is detected in permeate only at the higher temperature and concentration of CO_2, it is probable that the amount formed is too low to be detected in the continuous experiments of Fig. 8 at lower temperatures and CO_2 concentrations. It is thus mainly the reaction of CO_2 with specific sites, probably associated to defective positions in the boundary region of the grains. When the amount of subsurface O and/or C reaches saturation, the reaction progressively stops. Preliminary XPS studies confirm the presence of subsurface C in the thin films after reaction, but this analysis will be part of a consecutive paper on this topic.

The interpretation of the phenomenon is thus that CO_2 has a similar competitive effect on hydrogen dissociation in the two thin films, but in M1 the partial dissociation of CO_2 and reasonably O and/or C sublattice diffusion (enhanced in M1 with respect to M2 due to the nanostructure) combined with the lattice expansion due to H diffusion induces the presence of strains and microholes which favor the H_2 transport (together with other gases) through the thin film. Dissociation of CO_2 and the specific nanostructure are the two necessary conditions which determine the formation of reversible strains and microholes in M1 thin film.

Due to the presence of these reversible strains and microholes, an additional flux through the M1 thin film is present which partially compensates the inhibition by CO_2 chemisorption. For this reason, the large differences in the hydrogen fluxes using pure H_2 between M2 and M1 samples, is progressively reduced on increasing the CO_2 concentration in the feed (Fig. 8).

3.4. Characterization of the thin films after the tests in the presence of CO_2

Previous discussion has pointed out the concept of a reversible in situ modification of the characteristics of the Pd–Ag thin films, with creation of reversible strains and microholes particularly enhanced by the nanostructure present in M1 sample. These strains and microholes derive from the combined effect of CO_2 and of hydrogen diffusion through the thin film.When the flux of H_2 stops, there is a relatively rapid restoring of the initial situation. It

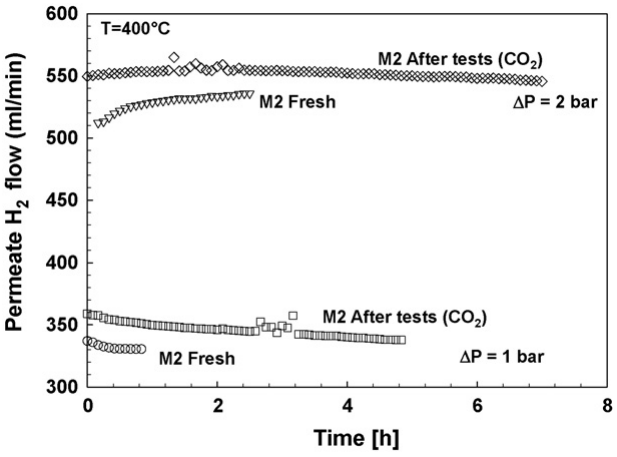

Fig. 10: Permeate flow of H_2 as a function of time-on-stream for 1 or 2 bar of differential pressure across the thin film for M2 thin film before and after the tests with the presence of CO_2 in the feed.

is thus evident that the characterization of the phenomenon requires operating in situ with the flow of hydrogen flowing through the membrane in the presence of CO_2, but this is technically quite challenging. Nevertheless, it may be interesting to analyze by electron microscopy the thin films after the tests with CO_2.

The results are summarized in Fig. 9 which report the SEM images (top view) of M1 and M2 thin films before and after the tests with CO_2. A microstructural evolution of the thin film may be observed with a desintering effect, e.g. with an increase of the surface instead of the minimization of the surface free energy. Note also that no evidences could be observed for the presence of surface carbon or carbon-like species.

Sudre and Lange [58] have modeled the effect of inclusions on the desintering phenomenon of ceramic powders. Their model concerned the breakup of grain bridges linking polycrystalline clusters. This breakup phenomenon results in the formation of large crack like voids. The mechanism that produces this breakup phenomenon (desintering) is a function of the grain size to bridge length ratio. When the ratio exceeds a critical value, the bridge will break up, e.g. disinter, to reduce the free energy of the system. This instability condition depends on the presence of inclusions in the bridge length or from stress conditions on the grain size. Reasonably the same considerations are valid also in our case. Therefore, the formation of subsurface O and/or C, and the stress induced from lattice expansion upon inclusion of hydrogen determine the desintering and the creation of crack like voids. In agreement with the presence of smaller grains, larger voids are observed by SEM in M1 sample after the tests with CO_2 with respect to M2 sample (Fig. 9). Therefore, even with the limits in the analysis mentioned above, SEM characterization of the samples confirms the previous conclusions.

However, it may be argued that apparently these SEM images do not indicate the reversibility of the formation of strains and microholes in the thin film. It is thus necessary to compare the permeability of the thin film in tests in pure H_2 before and after the tests with CO_2. The results for M2 thin film are shown in Fig. 10 and similar results were also observed for M1 sample. The behavior at two differential pressures across the thin film (1 or 2 bar) was measured.

Fig. 10 evidences that the permeate H_2 flow after the tests with CO_2 is slightly higher than that of the fresh sample, but only about 4% higher. Some permanent pinholes thus form, but in low amount, and do not justify thus the much higher differences observed in the tests with CO_2.

4. Conclusions

The use of co-deposition instead of sequential deposition during the preparation of Pd–Ag thin films by electroless plating deposition leads to two different nanostructures. The first sample shows a dendritic nanostructure, with the formation of one order magnitude smaller nanograins and higher surface roughness with respect to the sample prepared by sequential deposition. The latter has the typical dense characteristics of metallic thin films for H_2 separation, with a thickness of about 4–5μm. The permeability to H_2 of the thin films prepared by sequential deposition about 3–4 times higher than that of the sample prepared by co-deposition, which shows however a lower activation energy for hydrogen diffusion. Silver tends to accumulate at the boundary region between the grains. The presence of CO_2in the feed, however, changes considerably the performances and the behavior of the two thin films in hydrogen diffusion. The results indicate a reversible in situ modification of the characteristics of the Pd–Ag thin films, with creation of reversible strains and microholes particularly enhanced for th nanostructure present in the sample prepared by co-deposition (M1). These strains and microholes derive from the combined effect of CO_2 (with creation of subsurface O and/or C) and of hydrogen diffusion through the thin film, which induces lattice expansion and stress on the nanograins. When the flux of H_2 stops, there is a relatively rapid restoring of the initial situation. SEM characterization after the tests in the presence of CO_2 indicates the presence of desintering consistently with the above indications and the creation of crack like voids.

In conclusion, the results presented here evidence the original aspect that both the particular nanostructure and the presence of CO_2 in the feed (probably associated to the formation of subsurface O and/or carbon atoms) influence the properties and the nanomorphology of Pd–Ag thin films, and together with the presence of desintering phenomena. We feel that this is a more general phenomenon present also in other Pd-based bimetallic films and of more general interest to understand the performances and characteristics of Pd-based thin films which interest as membranes and catalysts is growing. The role of strains in determining the catalytic performances of supported Pd-alloy particles is under active discussion. Therefore, the results presented here open new aspects to understand the

catalytic reactivity of supported Pd-alloy catalysts, although this should be specifically investigated for these catalytic materials.

Acknowledgements

This work was realized in the frame of FISRMIUR project "H_2 puro da gas naturale mediante reforming a conversione totale ottenuta integrando reazione chimica e separazione a membrana" and of the EU Network of Excellence IDECAT (NMP3-CT-2005-011730).

References

[1] D. Barba, F. Giacobbe, A. De Cesaris, A. Farace, G. Iaquaniello, A. Pipino, Int. J. Hydrogen Energy 33 (14) (2008) 3700–3709.
[2] M. De Falco, D. Barba, S. Cosenza, G. Iaquaniello, A. Farace, F.G. Giacobbe, Asia-Pacific J. Chem. Eng. 4 (3) (2009) 259–269.
[3] G. Iaquaniello, F. Giacobbe, B. Morico, S. Cosenza, A. Farace, Int. J. Hydrogen Energy 33 (22) (2008) 6595–6601.
[4] M. De Falco, D. Barba, S. Cosenza, G. Iaquaniello, L. Marrelli, Int. J. Hydrogen Energy 33 (20) (2008) 5326–5334.
[5] A. Brunetti, G. Barbieri, E. Drioli, Chem. Eng. Sci. 64 (2009) 3448–3454.
[6] M.R. Rahimpour, H. Elekaei, Fuel Proc. Technol. 90 (2009) 747–761.
[7] A.A. Forghani, H. Elekaei, M.R. Rahimpour, Int. J. Hydrogen Energy 34 (2009) 3965–3976.
[8] A. Brunetti, G. Barbieri, E. Drioli, Chem. Eng. Proc. 47 (2008) 1081–1089.
[9] Ø. Hatlevik, S.K. Gade, M.K. Keeling, P.M. Thoen, A.P. Davidson, J.D. Way, Sep. Purif. Technol. 73 (2010) 59–64.
[10] S. Adhikari, S. Fernando, Ind. Eng. Chem. Res. 45 (3) (2006) 875–881.
[11] N.W. Ockwig, T.M. Nenoff, Chem. Rev. 107 (10) (2007) 4078–4110.
[12] H. Li, A. Goldbach, W. Li, H. Xu, J. Phys. Chem. B 112 (2008) 12182–12184.
[13] A.L. Mejdell, M. Jøndahl, T.A. Peters, R. Bredesen, H.J. Venvik, Sep. Purif. Technol. 68 (2009) 178–184.
[14] T.H. Nguyen, S. Mori, M. Suzuki, Chem. Eng. J. 155 (2009) 55–61.
[15] H. Li, A. Goldbach, W. Li, H. Xu, J. Membr. Sci. 299 (1–2) (2007) 130–137.
[16] F.C. Gielens, R.J.J. Knibbeler, P.F.J. Duysinx, H.D. Tong, M.A.G. Vorstman, J.T.F. Keurentjes, J. Membr. Sci. 279 (1–2) (2006) 176–185.
[17] D. Teschner, E. Vass, M. Hävecker, S. Zafeiratos, P. Schnörch, H. Sauea, A. Knop-Gericke, R. Schlögl, M. Chamam, A. Wootsch, A.S. Canning, J.J. Gamman, S.D.Jackson, J. McGregor, L.F. Gladden, J. Catal. 242 (1) (2006) 26–37.
[18] H. Gabasch, K. Hayek, B. Klötzer, A. Knop-Gericke, R. Schlögl, J. Phys. Chem. B 110 (10) (2006) 4947–4952.
[19] F. Studt, F. Abild-Pedersen, T. Bligaard, R.Z. Sørensen, C.H. Christensen, J.K. Nørskov, Angew. Chem. Int. Ed. 47 (48) (2008) 9299–9302.
[20] F. Viñes, C. Loschen, F. Illas, K.M. Neyman, J. Catal. 266 (1) (2009) 59–63.
[21] S. Nagarajan, K. Thirunavukkarasu, C.S. Gopinath, J. Phys. Chem. C 113 (17) (2009) 7385–7397.
[22] S. Penner, P. Bera, S. Pedersen, L.T. Ngo, J.J.W. Harris, C.T. Campbell, J. Phys. Chem. B 110 (48) (2006) 24577–24584.
[23] Y. Ma, F. Guazzone, Annales de Chimie: Sci. des Mat. 32 (2) (2007) 179–195.
[24] S.-K. Ryi, N. Xu, A. Li, C.J. Lim, J.R. Grace, Int. J. Hydrogen Energy 35 (6) (2010) 2328–2335.
[25] R. Bhandari, Y.H. Ma, J. Membr. Sci. 334 (1–2) (2009) 50–63.
[26] S. Abate, C. Genovese, S. Perathoner, G. Centi, Catal. Today 145 (2009) 63–71.
[27] H.-I. Chen, C.-Y. Chu, T.-C. Huang, J. Chin. Inst. Chem. Eng. 34 (1) (2003) 91–99.
[28] H.-I. Chen, C.-Y. Chu, T.-C. Huang, Thin Solid Films 460 (1–2) (2004) 62–71.
[29] H. Gao, Y.S. Lin, Y. Li, B. Zhang, Ind. Eng. Chem. Res. 43 (22) (2004) 6920–6930.
[30] A. Basile, F. Gallucci, S. Tosti, Membr. Sci. Technol. Ser. 13 (Inorganic Membranes) (2008) 255–323.
[31] D.A.P. Tanaka, M.A.L. Tanco, S.-i. Niwa, Y. oWakui, F. Mizukami, T. Namba, T.M. Suzuki, J. Membr. Sci. 247 (1–2) (2005) 21–27.
[32] W.-H. Lin, H.-F. Chang, Surf. Coat. Technol. 194 (1) (2005) 157–166.
[33] G. Strukul, R. Gavagnin, F. Pinna, E. Modaferri, S. Perathoner, G. Centi, M. Marella, M. Tomaselli, Catal. Today 55 (2000) 139–149.
[34] Y.X. Chen, Y. Zhang, H.Y. Liu, K.R. Sharma, G.H. Chen, Environ. Technol. 25 (2) (2004) 227–234.
[35] M.A. Hasnat, M.A. Islam, S.M. Borhanuddin, M.R.U. Chowdhury, M. Machida, J. Mol. Catal. A: Chem. 317 (1–2) (2010) 61–67.
[36] S. Melada, F. Pinna, G. Strukul, S. Perathoner, G. Centi, J. Catal. 235 (1) (2005) 241–248.
[37] S. Abate, G. Centi, S. Melada, S. Perathoner, F. Pinna, G. Strukul, Catal. Today 104 (2–4) (2005) 323–328.
[38] L. Shi, A. Goldbach, G. Zeng, H. Xu, J. Membr. Sci. 348 (1–2) (2010) 160–166.
[39] L. Wang, S. Bao, J. Yi, F. He, Z. Mi, Appl. Catal. B: Environ. 79 (2) (2008) 157–162.
[40] K. Sato, T.-a. Hanaoka, S. Hamakawa, M. Nishioka, K. Kobayashi, T. Inoue, T. Namba, F. Mizukami, Catal. Today 118 (1–2) (2006) 57–62.
[41] K. Sato, T.-A. Hanaoka, S.-I. Niwa, C. Stefan, T. Namba, F. Mizukami, Catal. Today 104 (2–4) (2005) 260–266.
[42] H. Orita, N. Itoh, Appl. Catal. A: Gen. 258 (1) (2004) 17–23.
[43] Y. Guo, X. Zhang, H. Zou, H. Liu, J. Wang, K.L. Yeung, Chem. Commun. (2009) 5898–5900.
[44] G. Centi, S. Perathoner, Catal. Today 143 (1–2) (2009) 145–150.
[45] J. Cizek, I. Prochazka, O. Melikhova,M.Vlach, N. Zaludova, G. Brauer,W.Anwand, W. Egger, P. Sperr, C. Hugenschmidt, R. Gemma, A. Pundt, R. Kirchheim, Physica Status Solidi C 6 (11) (2009) 2364–2366.
[46] S.C. Chen, C.C.Y. Hung, G.C. Tu, M.H. Rei, Int. J. Hydrogen Energy 33 (2008) 1880–1889.
[47] S. Abate, S. Perathoner, C. Genovese, G. Centi, Desalination 200 (1–3) (2006) 760–761.

[48] S. Abate, G. Centi, S. Perathoner, F. Frusteri, Catal. Today 118 (1–2) (2006) 189–197.
[49] S. Abate, G. Centi, S. Perathoner, C. Genovese, G. Iaquaniello, E. Lollobattista, Preprints—Am. Chem. Soc., Div. Petrol. Chem. 53 (1) (2008) 85–86.
[50] Y.S. Cheng, K.L. Yeung, J. Membr. Sci. 158 (1999) 127–141.
[51] G.L. Holleck, J. Phys. Chem. 74 (3) (1970) 503–511.
[52] R. Dittmeyer, V. Höllein, K. Daub, J. Mol. Catal. A 173 (2001) 135–184.
[53] J.W. Phair, R. Donelson, Ind. Eng. Chem. Res. 45 (2006) 5657–5674.
[54] W. Wang, X. Pan, X. Zhang, W. Yang, G. Xiong, Sep. Purif. Technol. 54 (2007) 171–262.
[55] V.P. Bushlanov, Nanotechnol. Russia 3 (5–6) (2008) 363–367.
[56] H. Barlag, L. Opara, H. Züchner, J. Alloys Compd. 330–332 (2002) 434–437.
[57] N. Mori, T. Nakamura, K.-i. Noda, O. Saki, A. Takahashi, Y. Iwamoto, T. Hattori, Ind. Eng. Chem. Res. 46 (2007) 1952–1958.
[58] O. Sudre, F.F. Lange, J. Am. Ceram. Soc. 75 (12) (2005) 3241–3251.